NANO LETTERS

pubs.acs.org/NanoLett

Letter

Nanoreporter Identifies Lysosomal Storage Disease Lipid Accumulation Intracranially

Merav Antman-Passig, Zvi Yaari, Dana Goerzen, Rooshi Parikh, Savannah Chatman, Lauren E. Komer, Chen Chen, Emma Grabarnik, Mickael Mathieu, Adriana Haimovitz-Friedman, and Daniel A. Heller*

Cite This: *Nano Lett.* 2023, 23, 10687−10695

Read Online

ACCESS | Metrics & More | Article Recommendations | Supporting Information

ABSTRACT: Dysregulated lipid metabolism contributes to neurodegenerative pathologies and neurological decline in lysosomal storage disorders as well as more common neurodegenerative diseases. Niemann−Pick type A (NPA) is a fatal neurodegenerative lysosomal storage disease characterized by abnormal sphingomyelin accumulation in the endolysosomal lumen. The ability to monitor abnormalities in lipid homeostasis intracranially could improve basic investigations and the development of effective treatment strategies. We investigated the carbon nanotube-based detection of intracranial lipid content. We found that the near-infrared emission of a carbon nanotube-based lipid sensor responds to lipid accumulation in neuronal and in vivo models of NPA. The nanosensor detected lipid accumulation intracranially in an acid sphingomyelinase knockout mouse via noninvasive near-infrared spectroscopy. This work indicates a tool to improve drug development processes in NPA, other lysosomal storage diseases, and neurodegenerative diseases.

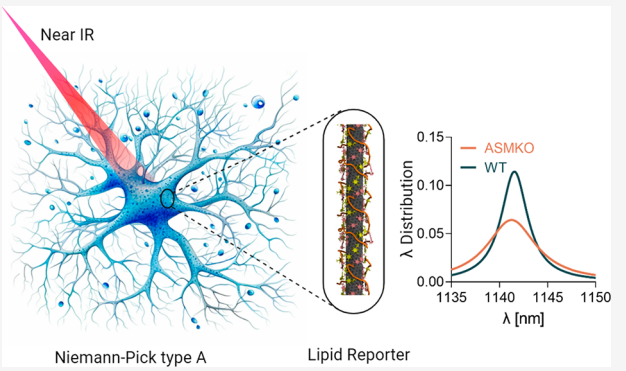

KEYWORDS: *biosensor, Niemann−Pick, sphingomyelin, neurodegenerative disease, carbon nanomaterials*

Lysosomal storage diseases are associated with abnormal accumulation of lipids in lysosomal compartments.[1] It is estimated that 70% of these diseases feature significant central nervous system (CNS) involvement.[2] Neuronal lysosomal lipid accumulation is associated with neurodegenerative lysosomal storage diseases including Gaucher disease,[3] Tay−Sachs disease,[4] and Niemann−Pick disease.

Niemann−Pick type A (NPA) disease is a rare, autosomal recessive lysosomal storage disorder characterized by hepatosplenomegaly and rapid neurodegeneration, ultimately leading to fatality during infancy. This neurodegenerative disorder is caused by the inherited deficiency in acid sphingomyelinase (ASM) activity, a lysosomal enzyme that hydrolyzes sphingomyelin (SM) into ceramide and phosphorylcholine. In NPA, loss-of-function mutations in the SMPD1 gene encoding ASM lead to the accumulation of SM within lysosomes in cells and tissues.[5] Indeed, studies performed on a knockout mouse model lacking ASM and with cells derived from patients show that intralysosomal accumulation of SM is a primary pathological event.[6] In the brain, the defective homeostasis of SM leads to neurodegeneration that initially affects Purkinje neurons in the cerebellum[7−9] and further involves astrogliosis, high oxidative stress, increased intracellular calcium,[10] and autophagy.[11] Neurons deficient in ASM are also characterized by increased SM in the plasma membrane, unpolarized distribution of proteins, dendritic spine anomalies,[12] and impaired synaptic vesicle docking.[13] Together, these effects highlight the importance of ASM for normal brain activity and may contribute to the pathological phenotype of cognitive deficits in NPA patients. The significant effect of ASM on neurological activity is also evident by the fact that minimal ASM activity, such as that in Niemann−Pick B patients, suffices to present mild to no neurological symptoms.[5] Identifying the effects and changes in ASM activity is therefore crucial for diagnosis, studying molecular abnormalities, and identifying therapeutic targets. Sensitive and reliable techniques for quantifying lysosomal SM, the primary pathological outcome of ASM deficiency (ASMD), are thus of considerable importance.

Direct quantification of ASM activity can be measured from serum or cerebrospinal fluid via measurements of fluorescent substrates metabolites[14,15] or mass spectrometry techniques[16] which allow for sensitive measurements of global lipid content.

Received: July 5, 2023
Revised: October 10, 2023
Published: October 27, 2023

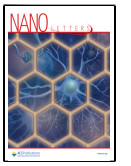

https://doi.org/10.1021/acs.nanolett.3c02502
Nano Lett. 2023, 23, 10687−10695

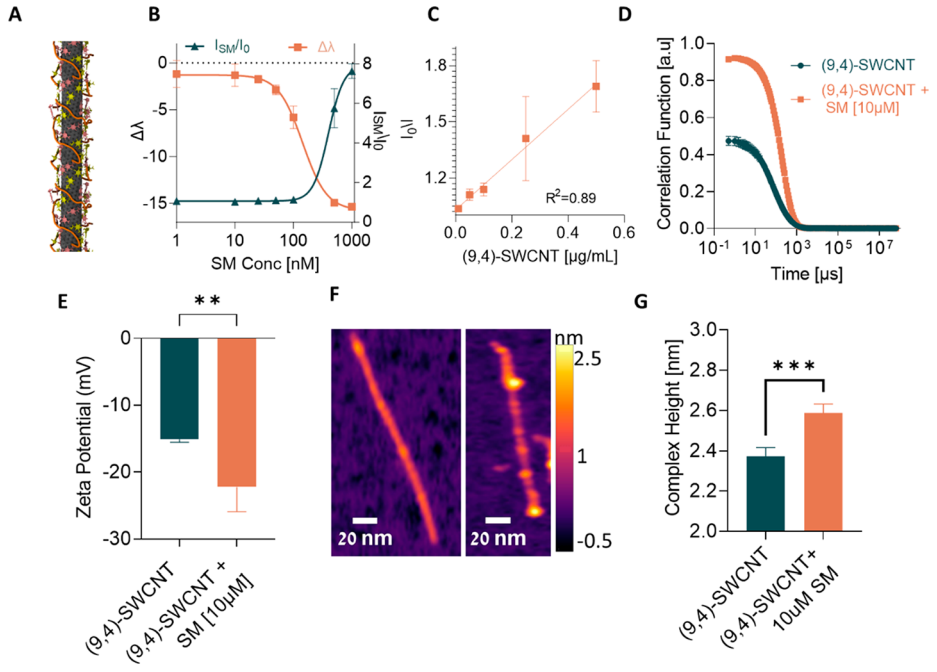

Figure 1. Characterization of the lipid reporter and sphingomyelin interaction. (A) Lipid reporter's optical reporter schematic. (B) Emission peak wavelength shift and intensity change of the lipid reporter nanotube complexes in solution as a function of SM concentration. n = 3, mean ± SD. (C) Stern−Volmer plot was derived for the quenching of C11-SM by the lipid reporter. n = 3, mean ± SD. (D) Correlograms from a dynamic light scattering instrument showing the correlation coefficient of the lipid reporter and the lipid reporter incubated with SM [10 μM] for 1 h at 37 °C. n = 3, mean ± SD. (E) Zeta-potential measurements of the lipid reporter and the lipid reporter incubated with SM [10 μM] for 1 h at 37 °C. n = 5, mean ± SD; $^{**}P < 0.01$, as measured via unpaired t test. (F) Representative AFM images of lipid reporters before (left) and after (right) the addition of SM. Scale bar: 20 nm. (G) Average height of the lipid reporter and the lipid reporter incubated with SM [10 μM] for 1 h at 37 °C, as derived from AFM images (n > 500 ridges). Mean ± SE, $^{***}p < 0.001$ as measured via unpaired t test.

However, these methods do not map the localization or compartmentalization of lipids. Specific localization and quantification of lipid content within lysosomes can be achieved via imaging techniques, such as fluorescent microscopy techniques. To fluorescently monitor SM, SM-binding proteins can be exploited to form fluorescent protein probes and can be used for studying lipid trafficking and metabolism.[17−19] Haberkant et al. suggested a method to fluorescently label SM by using a photoactivatable metabolic precursor of SM and using click chemistry in situ.[20] Alternatively, fluorophore-conjugated lipids can be used for imaging and studying lipid trafficking;[21] however, the conjugated fluorophore may change the native activity of the lipids.

The utilization of fluorescent imaging methodologies for the quantification of the SM content is laborious and impractical. To combine the qualities of rapid measurements of lipid content with localized-imaging capabilities, there is a need for an imaging reporter that can localize in lysosomes and provide quantitative data on lipid content rapidly. Moreover, despite the wealth of data regarding the molecular mechanisms that underlie NPA pathologies,[9] in vitro and cellular assays are insufficient to capture the extent of the effect of ASM deficiency on neurological impairments and aberrant brain phenotypes. To study the global impact of SM accumulation in the nervous system and to target preventative therapies, there is a need for lipid sensing modalities that can detect abnormal accumulation of SM directly in the brain.

Single-walled carbon nanotube (SWCNT) optical biosensors are cutting-edge technologies with unique features. Their intrinsic near-infrared-II (NIR-II) emission, ranging from 1000 to 1700 nm, aligns perfectly with the biological transparency window.[22] These biosensors offer exceptional photostability, minimal photobleaching, and no fluorescence intermittency, making them ideal for live brain tissue applications.[23] The NIR-II emission allows for deep optical penetration, reduced scattering, and low autofluorescence in biological tissues. Engineered SWCNTs, achieved through surface functionalization,[24−27] enable the detection of various biomolecules like protein biomarkers,[28,29] pH,[30] microRNA,[31] and lipids[32,33] in live cells.

In live brain tissue, SWCNT probes have successfully imaged neurotransmitters,[34] probed the extracellular space with low toxicity,[35,36] and detected amyloid beta.[37]

In this work, we endeavored to develop a biosensing technique that is capable of intracellular imaging and rapid and high-throughput measurements to monitor SM in brain and cell models. In the context of neurological disorders, a method to detect lysosomal lipid and SM accumulation intracranially can assist in the study of pathologies of diseases that exhibit abnormalities in the sphingolipid pathway. Here, we present a nanoreporter that optically monitors endolysosomal SM and lipid accumulation in vitro and from within the cerebellum *in vivo* in an ASMD model.

To develop a sensitive reporter for SM, we used intrinsic NIR fluorescence from single-walled carbon nanotubes (SWCNT) that were noncovalently complexed with single-stranded DNA (ssCTTC3TTC) (Figure 1A). We previously found the (9,4) chirality showed the greatest emission response to lipids and enabled endolysosomal localization without adversely affecting cell viability and organelle function.[32,33] Therefore, we enriched the nanotube reporter

https://doi.org/10.1021/acs.nanolett.3c02502
Nano Lett. 2023, 23, 10687−10695

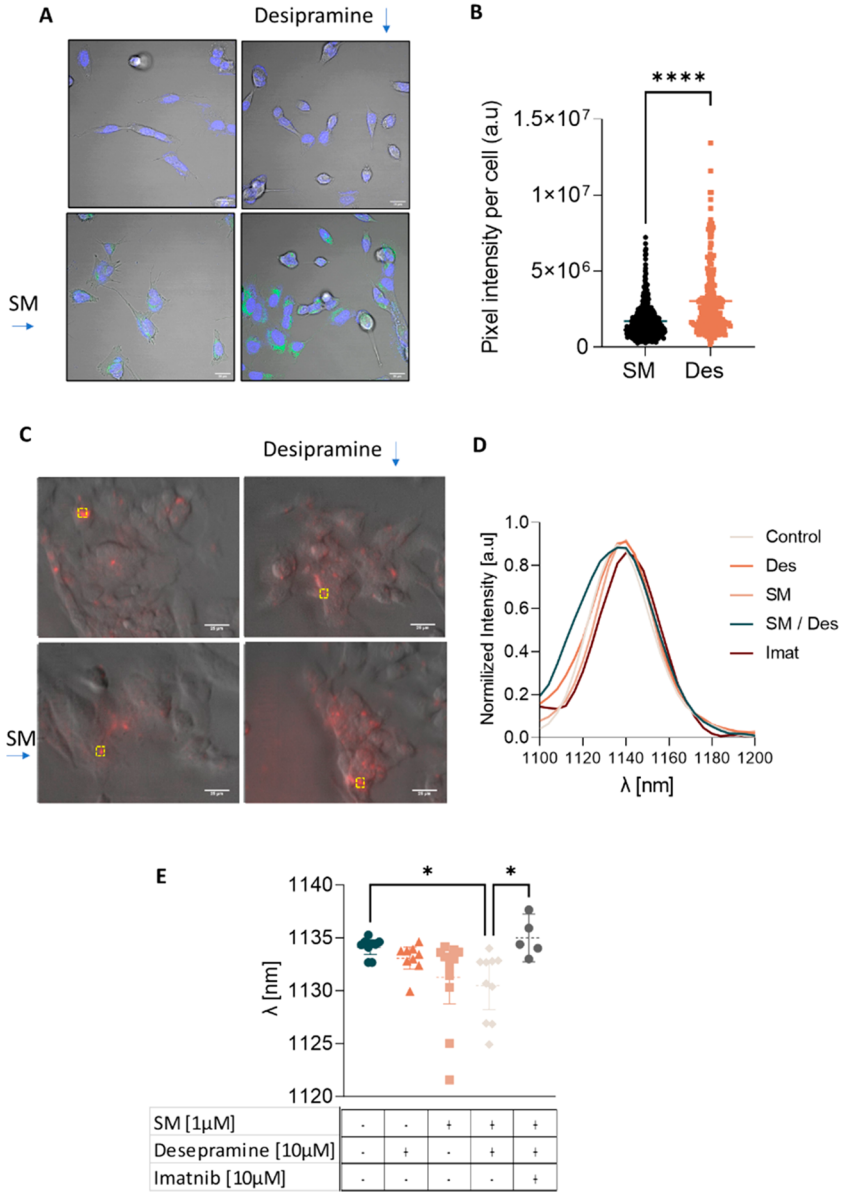

Figure 2. Lipid reporter detects SM accumulation in SHSY-5Y cells. (A) Representative fluorescence microscopy images of C11-SM [1 μM] (green) within SHSY-5Y cells treated with desipramine. Hoechst nuclei staining (blue). Scale bar: 20 μm. (B) C11-SM intensity profile per cell (n = 240), ****p < 0.0001 as measured via unpaired t test. (C) Representative bright-field images overlaid with near-infrared emission of ssCTTC3TTC-(9,4) SHSY-5Y cells. Scale bar: 25 μm. (D) Emission spectra of ROIs denoted in the images in panel C. Spectra were smoothed and normalized. (E) Center wavelength of the lipid reporter emission derived from well-plate (n = 10 from 2 individual biological experiments). *p < 0.05 as measured with a one-way ANOVA with Tukey's multiple comparisons test between groups (n > 5 wells).

with the (9,4) chirality via an aqueous two-phase (ATP) polymer separation system, a scalable method for chirality separation of DNA-wrapped SWCNTs.[38] We characterized the enrichment efficiency via absorbance following a one-step separation protocol and found comparable enrichment to previously reported separation[38] (Figure S1A,B). The enriched ssCTTC3TTC-(9,4) sensor responded to sphingomyelin (SM) in a decrease in center wavelength as a function of SM concentration (we henceforth denote ssCTTC3TTC-(9,4) sensor as lipid reporter) (Figure 1B). We note that in accordance with our previous reports,[32,33] the enrichment of the (9,4) chirality yields a larger change in central wavelength compared to unseparated solutions (Figure S1C). In our previous studies, we calculated that lipids, including sphingomyelin, bind to the reporter surface via hydrophobic interactions, increasing surface coverage on the nanotube surface and decreasing the water density in the nanotube's immediate vicinity. To study and validate this mechanism, we designed a set of experiments to study the surface interaction between the SM and the lipid reporter. First, we studied the effect the lipid reporter had on fluorescently labeled SM (C11-SM). We found the quenching of C11-SM by the lipid reporter, as described by a Stern−Volmer relationship, is close to linearity, suggesting that the majority of C11-SM and the lipid reporter are in close proximity, resulting in the deactivation of the fluorophore by energy transfer,[39] similar to effects of dye molecules in proximity to nanotubes (Figure 1C).[40−42] We note that the sensitivity of the fluorophore to quenching by the lipid reporter was higher following a 1 h incubation with SM, validating the importance of incubation

https://doi.org/10.1021/acs.nanolett.3c02502
Nano Lett. 2023, 23, 10687−10695

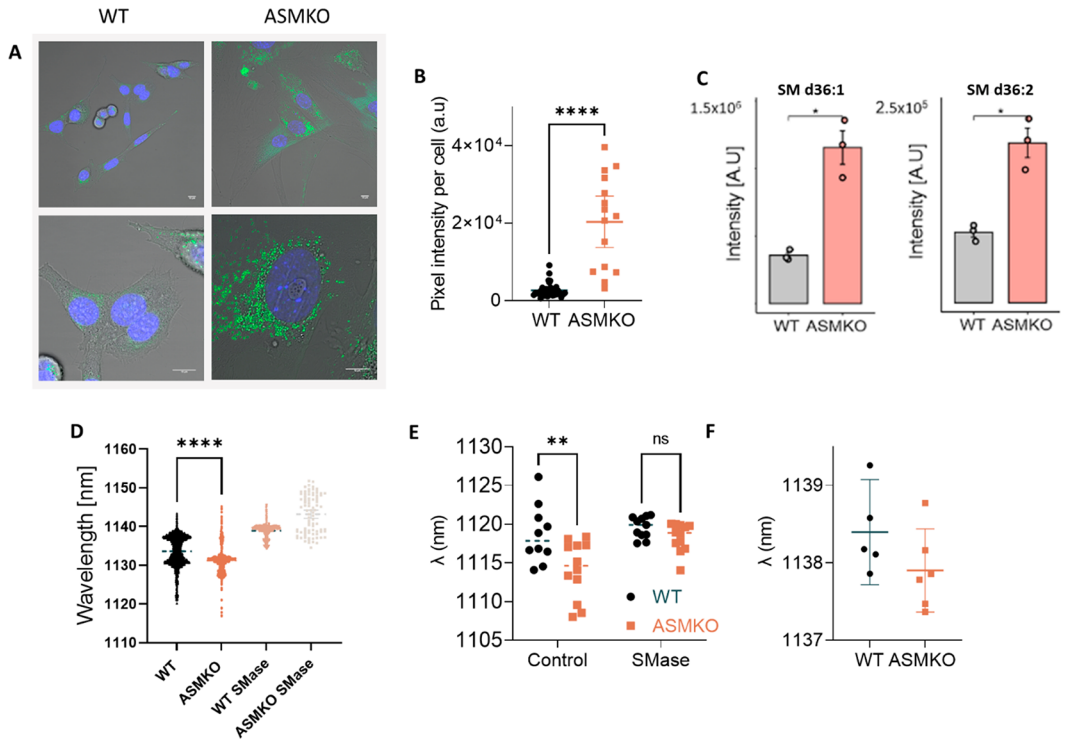

Figure 3. Lipid reporter detects SM in ASMKO MEF cells. (A) Representative fluorescence microscopy images of C11-SM [1 μM] (green) WT and ASMKO MEF cells. Hoechst nuclei staining (blue). Scale bar: 10 μm. (B) C11-SM intensity profile per cell (n = 16), ****p < 0.0001 as measured via unpaired t test. (C) Mass spectrometry analysis of 2 sphingomyelin species (SM d36:1, SMd36:2). *p < 0.05 as measured with Welch t test. (D) Center wavelength of the lipid reporter emission derived from hyperspectral imaging (n = 16). Error bars = standard error. ****p < 0.0001 as measured with a one-way ANOVA with Tukey's multiple comparisons test between groups. (E) Center wavelength of the lipid reporter emission derived from well-plate spectra (n = 10), **p < 0.01 as measured with a one-way ANOVA with Tukey's multiple comparisons test between groups (n = 10 wells). (F) Center wavelength of the lipid reporter emission from cell media.

with SM, to reach binding equilibrium between SM and the lipid reporter (Figure S1D). Next, we studied the surface chemistry changes of the reporter upon incubation with SM by monitoring the particle size via dynamic light scattering. Because SWCNTs are tubular, we used the correlation function derived from the dynamic light scattering of the lipid reporter, showing an increase and shift upon incubation with SM, suggesting an increase in nanotube size (Figure 1D). A decrease in zeta-potential suggests a greater charge density on the nanotube surfaces, indicating that charged SM is assigned to the surface of the nanotubes[43−45] (Figure 1E). Finally, the height profiles of the lipid reporter increased upon incubation with SM, as measured via AFM (Figures 1F,G and S2). Together, these experiments provide further evidence of the reporter mechanism in which SM is absorbed to the nanotube surfaces. Such proximity between hydrophobic molecules such as SM and nanotube surfaces changes the nanotube's local dielectric constant and photoluminescent energy shifts.[46,47]

We investigated the response of the lipid reporter to the lysosomal accumulation of SM in live ASMD cell models. We validated the reporter in a neuronal pharmacological cellular model, SH-SY5Y cells treated with an ASM inhibitor desipramine [10 μM].[48,49] We confirmed the NPA phenotype differential accumulation of C11-SM (Figure 2A,B). Upon incubation of the lipid reporter, local intracellular internalization was observed (Figure 2C).

Recent papers found that ASM deficiency is accompanied by autophagy lysosomal alterations.[11,50] A recent study found that c-Abl tyrosine kinase is activated in NPA models and downregulates autophagy, including in SH-SY5Y cells treated with desipramine.[48] Moreover, the authors found that treatment with imatinib, a clinical c-Abl inhibitor, restores autophagy flux[51] (Figure S3) and lowers sphingomyelin accumulation in NPA cell models. We therefore tested the effect of combined treatment of imatinib and desipramine on the reporter's wavelength emission. Spectra obtained from hyperspectral imaging of cells treated with desipramine and SM exhibited a distinct shifting of the emission compared to control groups (Figure 2D).

While the NIR hyperspectral microscopy enables visualization of the nanotube reporter localization, measurements in a high-throughput spectroscopy instrument can diminish the data acquisition time and enable fast screening of biologically distinct tests. In a high-throughput NIR spectroscopy instrument, the reporter showed a progressive decline in center wavelength emission upon incubation with SM, desipramine, and desipramine with SM (Figure 2E) from cells seeded in 96-well plates similar to hyperspectral single-pixel quantification. In agreement with the autophagy restoration function of imatinib, in our nanosensor experiments, we found that combined treatment with desipramine and imatinib increased the reporter's wavelength emission back to the baseline (Figure 2E).

We used the established genetic model for NPA mouse embryonic fibroblasts derived from ASM knockout mice (ASMKO MEF) for applying SM detection in NPA models. In agreement with the expected phenotype, ASMKO MEFs exhibit elevated accumulation of C11-SM in endolysosomal organelles, as visualized and quantified via fluorescence

https://doi.org/10.1021/acs.nanolett.3c02502
Nano Lett. 2023, 23, 10687−10695

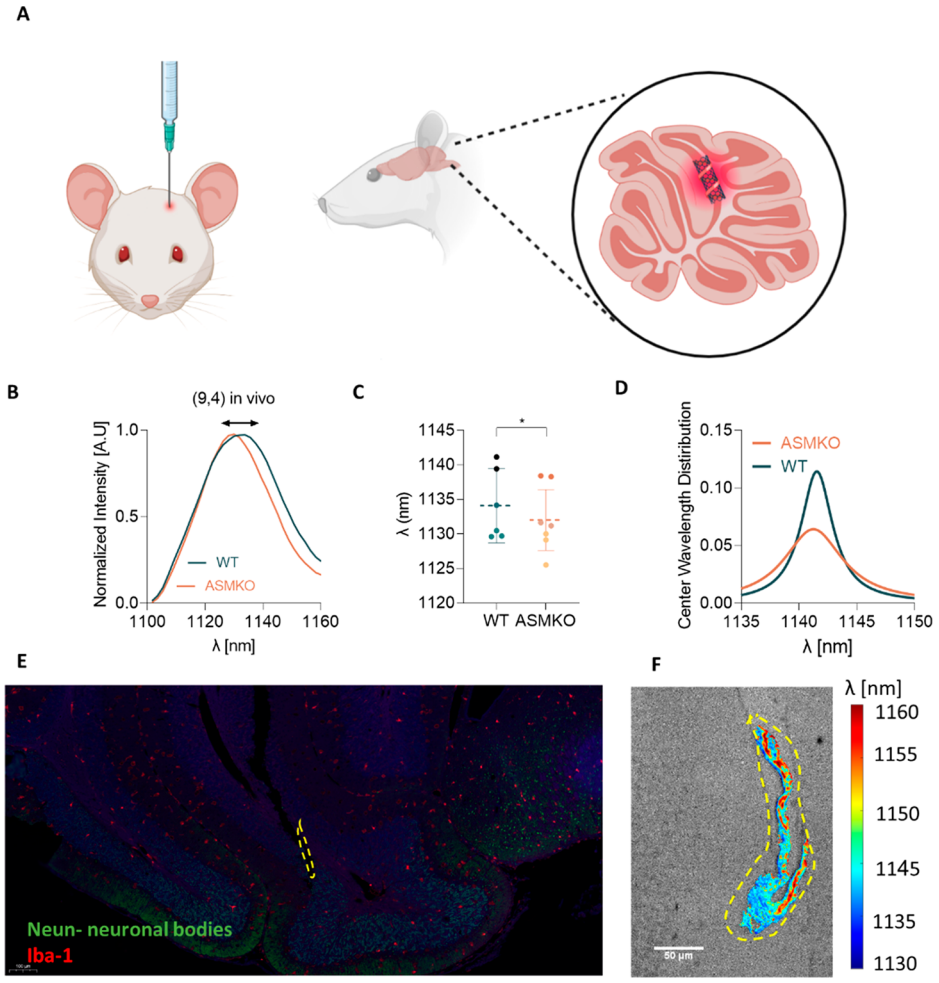

Figure 4. Lipid reporter identifies ASMKO mice model in vivo. (A) Schematic image of stereotaxic administration of the lipid reporter in the cerebellum (created with BioRender.com). (B) Representative emission spectra of the lipid reporter from mouse through-skull in vivo measurements. (C) Center wavelength of the lipid reporter emission from in vivo measurements. *$p < 0.05$ as measured with ANOVA test based on maximum likelihood ($n = 6$ mice, repeated experiment conducted in groups of 2 or 3 per group and are labeled in corresponding colors). (D) Representative emission spectra of the lipid reporter from cerebellum slices of WT and ASMKO mice. (E) Immunofluorescence image of the injection site in ASMKO mice cerebellum stained for neurons (NeuN, green), microglia (Iba-1, red), and nuclei (DAPI, blue). Injection site marked in yellow dashed lines. Scale bar: 50 μm. (F) Near-infrared hyperspectral map of reporter emission center wavelength overlaid with bright-field image in ASMKO mouse cerebellum, corresponding to panel E. Scale bar: 25 μm. Spectral bar: 1130−1160 nm.

microscopy (Figure 3A,B) and a global increase in two sphingomyelin species via mass spectrometry (Figure 3C). In addition to the increase in SM content, lipid measurements via mass spectrometry also revealed a decrease in ceramide levels in ASMKO MEFs, as compared to WT MEFs[52] (Figure S4).

We tested the capacity of the lipid reporter to visualize and account for elevated SM in live cells, without the necessity for adding external C11-SM. Following incubation with the lipid reporter, it localized intracellularly, and reporter spectra obtained from the ASMKO cells exhibited a distinct shifting of the emission compared with WT (Figure S5). Violin plots obtained from single-pixel NIR hyperspectral microscopy[53] of the reporter from within ASMKO cells showed a shifted population by ∼5 nm compared to WT. Moreover, upon treatment with SMase, the emission returned to a baseline similar to WT (Figure 3D). In a high-throughput NIR spectroscopy instrument, the reporter delivered similar trends from cells seeded in 96-well plates to hyperspectral single-pixel quantification (Figure 3E).

In NPA, together with the abnormal accumulation of lipids in lysosomes, an increase in extracellular lipids is observed[54,55] (Figure S6). Therefore, we tested the sensitivity of the reporter for detecting differences in the extracellular lipids. The overall average center wavelength was lower by ∼0.5 nm in media extracted from ASMKO MEF cell culture as compared to media extracted from WT MEF cells (Figure 3F). This change in magnitude ($\Delta\lambda \sim 5$ nm detected from within live cells) can reflect a lower difference in lipid content in cell media. Alternatively, it can be attributed to nonspecific interactions with proteins, nutrients, or salts that can attenuate the effectiveness of the signal. To determine whether such nonspecific protein interactions were associated with the change in center wavelength observed in the media extracted from ASMKO cell culture, we assessed the total protein content with data from the reporter emission and found no significant correlation (Figure S7).

To locally detect SM accumulation in the cerebellum, the initially affected brain region,[8] we administered the lipid reporter directly in mice cerebellum via stereotaxic injection

https://doi.org/10.1021/acs.nanolett.3c02502
Nano Lett. 2023, 23, 10687−10695

(Figure 4A,B). We used an ASM knockout (ASMKO) transgenic mouse model that expresses NPA phenotypes including neurodegeneration.[9,56] Spectra recorded through intact cranium from the cerebellum region were compared between the ASMKO and WT mice. In all experiments (marked as colored dots), a decrease in the central wavelength of the reporter in ASMKO mice as compared to WT mice was noted (Figure 4C), indicating higher lipid content in the knockout mice.

To investigate the fate of the nanosensors in the cerebellum, we resected tissue and used NIR microscopy to identify the emission of the nanotubes. NIR hyperspectral microscopy was conducted on the tissues, showing a decrease in center wavelength in ASMKO samples as compared to WT tissues (Figure 4D). In resected cerebellar tissue from mice injected with the sensor, we found a substantial number of nanotubes near the injection site (Figure 4E,F). We noted that injecting the nanosensors into the cerebellum did not induce significant cell damage (Figure S8), indicating relative biocompatibility for functional sensing of lipid accumulation from within brain tissues in vivo.

Herein, we describe the detection of neuropathological SM accumulation in vitro and in vivo. Central to this method was the development of a biocompatible[57] nanosensor for detection of cholesterol and SM, consisting of (9,4) SWCNTs noncovalently complexed with the single-stranded oligonucleotide CTTC3TTC, as described in our previous reports.[32,33] In our previous results, we showed that the optical shift correlated to dielectric environment of the nanotube surfaces. Based on the new findings from our experiments, we corroborated the mechanism proposed previously and determined that SM absorbs on nanotube surfaces, inducing a change in the local dielectric constant and photoluminescent energy shifts. Lipid binding to a nanotube surface is governed by the hydrophobic, electrostatic, and amphiphilic properties of the lipids, properties which may contribute to the optical shift of the reporter in response to different lipid species. We observed the nanosensor response to SM in live NPA cells and mouse models. We used the nanosensor to report the retrieval of normal ASM activity in cell models, validating the potential of the nanosensor for the development of NPA therapies. With this in mind, we investigated a method for screening cells in 96-well plates, indicating the amenability of the sensor for both imaging spectroscopy-based assays that facilitate higher throughput measurements.[33] The therapeutic treatments that we used for in vitro studies, such as imatinib, show limited effects in vivo due to poor penetration through the BBB[58,59] and were neglected in this study for in vivo use. In future studies, screening for new NPA therapies in vivo could potentially accelerate diagnostic testing processes by providing relative brain SM valuation in a rapid and direct method.

We aim to develop a method capable of detecting lipid dysregulation in the brain, as such measurements remain a challenge.[60] The efficiency of the nanotube-based reporter to target and identify endolysosomal lipid accumulation in the liver was established in previous reports.[33] Following IP injection, the reporter localizes mainly to the liver and is confined to lysosomal compartments in Kupffer cells.[33,57] We also previously found that following i.v. administration of SWCNTs the small amounts that cross the BBB do not allow for optical detection of sensors in live samples.[57] Here, we found that the injection of carbon nanotube sensors directly into the cerebellum results in a local extracellular pool of nanotubes in the brain. Extracellular accumulation of nanotube sensors has been reported following intracranial injections[37] and observed in ex vivo preparations.[35,36,61,62] Following intracerebral injection, the sensor localized in extracellular pools and responded in ASMKO mice by a decrease in the average center wavelength. Although the nanosensor did not directly detect lysosomal accumulation of SM, it is possible that the change in signal is due to secondary effects of aberrant SM metabolism, such as increased SM levels in neuronal plasma membranes,[63,64] altered lipid composition,[64] increased CSF SM,[65] or adjuvant mechanisms.[66] Extralysosomal lipids can be detected via the sensor, as demonstrated in the solution and from media extracted from ASMKO MEF cells. Although collecting CSF from ASMKO mice would have been preferable to determine the in vivo mechanism, obtaining sufficient CSF from mice is challenging. Whether the contact between nanosensors and SM occurs at the interface with SM-rich plasma membranes or by interaction with SM circulating the CSF in nanoscaled structures such as exosomes, synaptic vesicles, or dense core vesicles[67,68] is yet unknown. Nonetheless, global identification of ASM deficiencies and subsequent SM accumulation at the cerebellum level are beneficial for studying disease progression and drug development applications. For example, the sensor can be used intracranially to assess the degree of pathology in ASMD live mice at different brain regions or different stages.[8] The nanosensor can also be applied in ASMD in vitro models to investigate molecular mechanisms that may be responsible for neurological dysfunction and as complementary tools for investigating the lysosomal environment.[30] Additionally, the nanosensor can be applied to study abnormalities in ASM activity in other neurological disorders,[69] such as Alzheimer's disease.[70] One potential limitation of this nanosensor is the broad susceptibility to non-SM lipids such as cholesterol. This drawback can be mitigated with the selective use of lipidomic assays that can clarify the lipid profile distributions.

■ ASSOCIATED CONTENT

Supporting Information

The Supporting Information is available free of charge at https://pubs.acs.org/doi/10.1021/acs.nanolett.3c02502.

Characterization of the lipid reporter, lipidomic profiling of ASMKO MEF cells; nanosensor detection of lipid accumulation in ASMKO MEF (PDF)

Materials and Methods (PDF)

■ AUTHOR INFORMATION

Corresponding Author

Daniel A. Heller − *Memorial Sloan Kettering Cancer Center, New York, New York 10065, United States; Weill Cornell Medicine, Cornell University, New York, New York 10065, United States;* orcid.org/0000-0002-6866-0000; Email: hellerd@mskcc.org

Authors

Merav Antman-Passig − *Memorial Sloan Kettering Cancer Center, New York, New York 10065, United States;* orcid.org/0000-0003-2102-9139

Zvi Yaari − *Memorial Sloan Kettering Cancer Center, New York, New York 10065, United States;* Present Address: School of Pharmacy, Faculty of Medicine, The

https://doi.org/10.1021/acs.nanolett.3c02502
Nano Lett. 2023, 23, 10687−10695

Hebrew University of Jerusalem, Jerusalem 9112102, Israel

Dana Goerzen − *Memorial Sloan Kettering Cancer Center, New York, New York 10065, United States; Weill Cornell Medicine, Cornell University, New York, New York 10065, United States*

Rooshi Parikh − *The City College of New York, New York, New York 10031, United States*

Savannah Chatman − *Department of Biomedical Engineering, Washington University in St. Louis, St. Louis, Missouri 63130, United States; Engineering Program, Scripps College, Claremont, California 91711, United States*

Lauren E. Komer − *Helen and Robert Appel Alzheimer's Disease Research Institute, Brain and Mind Research Institute, Weill Cornell Medicine, New York, New York 10065, United States*

Chen Chen − *Memorial Sloan Kettering Cancer Center, New York, New York 10065, United States; Weill Cornell Medicine, Cornell University, New York, New York 10065, United States; Tri-Institutional PhD Program in Chemical Biology, Memorial Sloan Kettering Cancer Center, New York, New York 10065, United States*

Emma Grabarnik − *Memorial Sloan Kettering Cancer Center, New York, New York 10065, United States*

Mickael Mathieu − *Department of Radiation Oncology, Memorial Sloan Kettering Cancer Center, New York, New York 10065, United States;* Present Address: Clinical Research Unit, Emile Roux Hospital Center, Le Puy-en-Velay 43000, France.

Adriana Haimovitz-Friedman − *Department of Radiation Oncology, Memorial Sloan Kettering Cancer Center, New York, New York 10065, United States*

Complete contact information is available at: https://pubs.acs.org/10.1021/acs.nanolett.3c02502

Funding

This work was supported in part by the NCI (Cancer Center Support Grant P30-CA008748), NINDS (R01-NS116353 R01-NS122987), the National Science Foundation CAREER Award (1752506), the Ara Parseghian Medical Research Fund, the Expect Miracles Foundation - Financial Services Against Cancer, the Louis and Rachel Rudin Foundation, Emerson Collective, MSK's Cycle for Survival's Equinox Innovation Award in Rare Cancers, Mr. William H. Goodwin and Mrs. Alice Goodwin and the Commonwealth Foundation for Cancer Research, and the Experimental Therapeutics Center of Memorial Sloan Kettering Cancer Center. R.P was supported by NIH Grant (U54CA132378). Z.Y. was supported by the Ann Schreiber Mentored Investigator Award (Ovarian Cancer Research Fund) and Young Investigator 2019 (Kaleidoscope of Hope). M.A.P. was supported by the Joe W. and Dorothy Dorsett Brown Foundation.

Notes

The authors declare the following competing financial interest(s): D.A.H. is a co-founder and officer with an equity interest in Lime Therapeutics Inc., a co-founder with an equity interest in Selectin Therapeutics Inc., and Resident Diagnostics, Inc., and a member of the scientific advisory board of Concarlo Therapeutics, Inc., Nanorobotics Inc., and Mediphage Bioceuticals Inc.

ACKNOWLEDGMENTS

We thank the Richard Kolesnick Lab for their generous gift of ASMKO MEF cells and special thanks to Tambudzai Shamu for technical assistance. We thank Prakrit Jena for the image analysis code and fruitful discussions, and Prakrit Jena and Daniel Roxbury for thier assistance with images. We thank Zhigang Zhang from the Epidemiology-Biostatistics department for helping with statistical analysis of animal studies. We thank the staff of the Molecular Cytology Core Facility (MCCF) at Memorial Sloan Kettering Cancer Center for AFM imaging, live-cell confocal microscopy, and tissue sectioning and preparation. We especially acknowledge Biran Wang, Afsar Barlas, Ning Fan, Yevgeniy Romin, and Eric Chan. We thank Michelle Saoi from the Donald B. and Catherine C. Marron Cancer Metabolism Center at Memorial Sloan Kettering for the lipidomic profiling.

REFERENCES

(1) Parini, R.; Andria, G. Lysosomal Storage Diseases; John Libbey Eurotext, 2010.

(2) Wraith, J. E. The Clinical Presentation of Lysosomal Storage Disorders. *Acta Neurol. Taiwan* **2004**, *13* (3), 101−106.

(3) Aerts, J. M. F. G.; Kuo, C.-L.; Lelieveld, L. T.; Boer, D. E. C.; van der Lienden, M. J. C.; Overkleeft, H. S.; Artola, M. Glycosphingolipids and Lysosomal Storage Disorders as Illustrated by Gaucher Disease. *Curr. Opin. Chem. Biol.* **2019**, *53*, 204−215.

(4) Fernandes Filho, J. A.; Shapiro, B. E. Tay-Sachs Disease. *Arch. Neurol.* **2004**, *61* (9), 1466−1468.

(5) Schuchman, E. H.; Wasserstein, M. P. Types A and B Niemann-Pick Disease. *Pediatr. Endocrinol. Rev.* **2016**, *13* (Suppl 1), 674−681.

(6) Pfrieger, F. W. The Niemann-Pick Type diseases-A Synopsis of Inborn Errors in Sphingolipid and Cholesterol Metabolism. *Prog. Lipid Res.* **2023**, *90*, 101225.

(7) Otterbach, B.; Stoffel, W. Acid Sphingomyelinase-Deficient Mice Mimic the Neurovisceral Form of Human Lysosomal Storage Disease (Niemann-Pick Disease). *Cell* **1995**, *81* (7), 1053−1061.

(8) Macauley, S. L.; Sidman, R. L.; Schuchman, E. H.; Taksir, T.; Stewart, G. R. Neuropathology of the Acid Sphingomyelinase Knockout Mouse Model of Niemann-Pick A Disease Including Structure-function Studies Associated with Cerebellar Purkinje Cell Degeneration. *Exp. Neurol.* **2008**, *214*, 181−192.

(9) Ledesma, M. D.; Prinetti, A.; Sonnino, S.; Schuchman, E. H. Brain Pathology in Niemann Pick Disease Type A: Insights from the Acid Sphingomyelinase Knockout Mice. *J. Neurochem.* **2011**, *116* (5), 779−788.

(10) Pérez-Cañamás, A.; Benvegnù, S.; Rueda, C. B.; Rábano, A.; Satrústegui, J.; Ledesma, M. D. Sphingomyelin-Induced Inhibition of the Plasma Membrane Calcium ATPase Causes Neurodegeneration in Type A Niemann-Pick Disease. *Mol. Psychiatry* **2017**, *22* (5), 711−723.

(11) Gabandé-Rodríguez, E.; Boya, P.; Labrador, V.; Dotti, C. G.; Ledesma, M. D. High Sphingomyelin Levels Induce Lysosomal Damage and Autophagy Dysfunction in Niemann Pick Disease Type A. *Cell Death Differ.* **2014**, *21* (6), 864−875.

(12) Arroyo, A. I.; Camoletto, P. G.; Morando, L.; Sassoe-Pognetto, M.; Giustetto, M.; Van Veldhoven, P. P.; Schuchman, E. H.; Ledesma, M. D. Pharmacological Reversion of Sphingomyelin-Induced Dendritic Spine Anomalies in a Niemann Pick Disease Type A Mouse Model. *EMBO Mol. Med.* **2014**, *6* (3), 398−413.

(13) Camoletto, P. G.; Vara, H.; Morando, L.; Connell, E.; Marletto, F. P.; Giustetto, M.; Sassoè-Pognetto, M.; Van Veldhoven, P. P.; Ledesma, M. D. Synaptic Vesicle Docking: Sphingosine Regulates syntaxin1 Interaction with Munc18. *PLoS One* **2009**, *4* (4), e5310.

(14) He, X.; Chen, F.; Dagan, A.; Gatt, S.; Schuchman, E. H. A Fluorescence-Based, High-Performance Liquid Chromatographic Assay to Determine Acid Sphingomyelinase Activity and Diagnose

Types A and B Niemann-Pick Disease. *Anal. Biochem.* **2003**, *314*, 116−120.
(15) Mühle, C.; Huttner, H. B.; Walter, S.; Reichel, M.; Canneva, F.; Lewczuk, P.; Gulbins, E.; Kornhuber, J. Characterization of Acid Sphingomyelinase Activity in Human Cerebrospinal Fluid. *PLoS One* **2013**, *8* (5), e62912.
(16) Züllig, T.; Köfeler, H. C. High Resolution Mass Spectrometry In Lipodomics. *Mass Spectrom. Rev.* **2021**, *40* (3), 162−176.
(17) Holthuis, J. C. M.; Menon, A. K. Lipid Landscapes and Pipelines in Membrane Homeostasis. *Nature* **2014**, *510* (7503), 48−57.
(18) Deng, Y.; Rivera-Molina, F. E.; Toomre, D. K.; Burd, C. G. Sphingomyelin Is Sorted at the Trans Golgi Network into a Distinct Class of Secretory Vesicle. *Proc. Natl. Acad. Sci. U. S. A.* **2016**, *113* (24), 6677−6682.
(19) Shogomori, H.; Kobayashi, T. Lysenin: A Sphingomyelin Specific Pore-Forming Toxin. *Biochim. Biophys. Acta* **2008**, *1780* (3), 612−618.
(20) Haberkant, P.; Stein, F.; Höglinger, D.; Gerl, M. J.; Brügger, B.; Van Veldhoven, P. P.; Krijgsveld, J.; Gavin, A.-C.; Schultz, C. Bifunctional Sphingosine for Cell-Based Analysis of Protein-Sphingolipid Interactions. *ACS Chem. Biol.* **2016**, *11* (1), 222−230.
(21) Maxfield, F. R.; Wüstner, D. Analysis of Cholesterol Trafficking with Fluorescent Probes. *Methods Cell Biol.* **2012**, *108*, 367−393.
(22) Barone, P. W.; Baik, S.; Heller, D. A.; Strano, M. S. Near-Infrared Optical Sensors Based on Single-Walled Carbon Nanotubes. *Nat. Mater.* **2005**, *4* (1), 86−92.
(23) Weisman, R. B.; Kono, J. FRONT MATTER. In *Handbook of Carbon Nanomaterials*; World Scientific Series on Carbon Nanoscience; World Scientific: 2017; Vols. *9* and *10*, pp i−xxxvi.
(24) Yaari, Z.; Yang, Y.; Apfelbaum, E.; Cupo, C.; Settle, A. H.; Cullen, Q.; Cai, W.; Roche, K. L.; Levine, D. A.; Fleisher, M.; Ramanathan, L.; Zheng, M.; Jagota, A.; Heller, D. A. A Perception-Based Nanosensor Platform to Detect Cancer Biomarkers. *Sci. Adv.* **2021**, *7* (47), eabj0852.
(25) Kim, M.; Chen, C.; Wang, P.; Mulvey, J. J.; Yang, Y.; Wun, C.; Antman-Passig, M.; Luo, H.-B.; Cho, S.; Long-Roche, K.; Ramanathan, L. V.; Jagota, A.; Zheng, M.; Wang, Y.; Heller, D. A. Detection of Ovarian Cancer via the Spectral Fingerprinting of Quantum-Defect-Modified Carbon Nanotubes in Serum by Machine Learning. *Nat. Biomed. Eng.* **2022**, *6* (3), 267−275.
(26) Zhang, J.; Landry, M. P.; Barone, P. W.; Kim, J.-H.; Lin, S.; Ulissi, Z. W.; Lin, D.; Mu, B.; Boghossian, A. A.; Hilmer, A. J.; Rwei, A.; Hinckley, A. C.; Kruss, S.; Shandell, M. A.; Nair, N.; Blake, S.; Şen, F.; Şen, S.; Croy, R. G.; Li, D.; Yum, K.; Ahn, J.-H.; Jin, H.; Heller, D. A.; Essigmann, J. M.; Blankschtein, D.; Strano, M. S. Molecular Recognition Using Corona Phase Complexes Made of Synthetic Polymers Adsorbed on Carbon Nanotubes. *Nat. Nanotechnol.* **2013**, *8* (12), 959−968.
(27) Gerstman, E.; Hendler-Neumark, A.; Wulf, V.; Bisker, G. Monitoring the Formation of Fibrin Clots as Part of the Coagulation Cascade Using Fluorescent Single-Walled Carbon Nanotubes. *ACS Appl. Mater. Interfaces* **2023**, *15* (18), 21866−21876.
(28) Williams, R. M.; Lee, C.; Galassi, T. V.; Harvey, J. D.; Leicher, R.; Sirenko, M.; Dorso, M. A.; Shah, J.; Olvera, N.; Dao, F.; Levine, D. A.; Heller, D. A. Noninvasive Ovarian Cancer Biomarker Detection via an Optical Nanosensor Implant. *Sci. Adv.* **2018**, *4* (4), eaaq1090.
(29) Ehrlich, R.; Hendler-Neumark, A.; Wulf, V.; Amir, D.; Bisker, G. Optical Nanosensors for Real-Time Feedback on Insulin Secretion by *β*-Cells. *Small* **2021**, *17* (30), e2101660.
(30) Kim, M.; Chen, C.; Yaari, Z.; Frederiksen, R.; Randall, E.; Wollowitz, J.; Cupo, C.; Wu, X.; Shah, J.; Worroll, D.; Lagenbacher, R. E.; Goerzen, D.; Li, Y.-M.; An, H.; Wang, Y.; Heller, D. A. Nanosensor-Based Monitoring of Autophagy-Associated Lysosomal Acidification in Vivo. *Nat. Chem. Biol.* **2023**, 1−10.
(31) Harvey, J. D.; Jena, P. V.; Baker, H. A.; Zerze, G. H.; Williams, R. M.; Galassi, T. V.; Roxbury, D.; Mittal, J.; Heller, D. A. A Carbon Nanotube Reporter of miRNA Hybridization Events In Vivo. *Nat. Biomed. Eng.* **2017**, *1* (4), 0041.
(32) Jena, P. V.; Roxbury, D.; Galassi, T. V.; Akkari, L.; Horoszko, C. P.; Iaea, D. B.; Budhathoki-Uprety, J.; Pipalia, N.; Haka, A. S.; Harvey, J. D.; Mittal, J.; Maxfield, F. R.; Joyce, J. A.; Heller, D. A. A Carbon Nanotube Optical Reporter Maps Endolysosomal Lipid Flux. *ACS Nano* **2017**, *11* (11), 10689−10703.
(33) Galassi, T. V.; Jena, P. V.; Shah, J.; Ao, G.; Molitor, E.; Bram, Y.; Frankel, A.; Park, J.; Jessurun, J.; Ory, D. S.; Haimovitz-Friedman, A.; Roxbury, D.; Mittal, J.; Zheng, M.; Schwartz, R. E.; Heller, D. A. An Optical Nanoreporter of Endolysosomal Lipid Accumulation Reveals Enduring Effects of Diet on Hepatic Macrophages in Vivo. *Sci. Transl. Med.* **2018**, *10* (461), eaar2680.
(34) Yang, S. J.; Del Bonis-O'Donnell, J. T.; Beyene, A. G.; Landry, M. P. Near-Infrared Catecholamine Nanosensors for High Spatiotemporal Dopamine Imaging. *Nat. Protoc.* **2021**, *16* (6), 3026−3048.
(35) Paviolo, C.; Soria, F. N.; Ferreira, J. S.; Lee, A.; Groc, L.; Bezard, E.; Cognet, L. Nanoscale Exploration of the Extracellular Space in the Live Brain by Combining Single Carbon Nanotube Tracking and Super-Resolution Imaging Analysis. *Methods* **2020**, *174*, 91−99.
(36) Godin, A. G.; Varela, J. A.; Gao, Z.; Danné, N.; Dupuis, J. P.; Lounis, B.; Groc, L.; Cognet, L. Single-Nanotube Tracking Reveals the Nanoscale Organization of the Extracellular Space in the Live Brain. *Nat. Nanotechnol.* **2017**, *12* (3), 238−243.
(37) Antman-Passig, M.; Wong, E.; Frost, G. R.; Cupo, C.; Shah, J.; Agustinus, A.; Chen, Z.; Mancinelli, C.; Kamel, M.; Li, T.; Jonas, L. A.; Li, Y.-M.; Heller, D. A. Optical Nanosensor for Intracellular and Intracranial Detection of Amyloid-Beta. *ACS Nano* **2022**, *16* (5), 7269−7283.
(38) Lyu, M.; Meany, B.; Yang, J.; Li, Y.; Zheng, M. Toward Complete Resolution of DNA/Carbon Nanotube Hybrids by Aqueous Two-Phase Systems. *J. Am. Chem. Soc.* **2019**, *141* (51), 20177−20186.
(39) Lakowicz, J. R. *Principles of Fluorescence Spectroscopy*; Springer Science & Business Media: 2013.
(40) Yang, R.; Jin, J.; Chen, Y.; Shao, N.; Kang, H.; Xiao, Z.; Tang, Z.; Wu, Y.; Zhu, Z.; Tan, W. Carbon Nanotube-Quenched Fluorescent Oligonucleotides: Probes That Fluoresce upon Hybridization. *J. Am. Chem. Soc.* **2008**, *130* (26), 8351−8358.
(41) Pinals, R. L.; Ledesma, F.; Yang, D.; Navarro, N.; Jeong, S.; Pak, J. E.; Kuo, L.; Chuang, Y.-C.; Cheng, Y.-W.; Sun, H.-Y.; Landry, M. P. Rapid SARS-CoV-2 Spike Protein Detection by Carbon Nanotube-Based Near-Infrared Nanosensors. *Nano Lett.* **2021**, *21* (5), 2272−2280.
(42) Chiu, C. F.; Dementev, N.; Borguet, E. Fluorescence Quenching of Dyes Covalently Attached to Single-Walled Carbon Nanotubes. *J. Phys. Chem. A* **2011**, *115* (34), 9579−9584.
(43) Kamble, S.; Agrawal, S.; Cherumukkil, S.; Sharma, V.; Jasra, R. V.; Munshi, P. Revisiting Zeta Potential, the Key Feature of Interfacial Phenomena, with Applications and Recent Advancements. *ChemistrySelect* **2022**, *7* (1), e202103084.
(44) Brown, M. A.; Goel, A.; Abbas, Z. Effect of Electrolyte Concentration on the Stern Layer Thickness at a Charged Interface. *Angew. Chem., Int. Ed. Engl.* **2016**, *55* (11), 3790−3794.
(45) Chang, Q. *Colloid and Interface Chemistry for Water Quality Control*; Elsevier Science: 2016.
(46) Larsen, B. A.; Deria, P.; Holt, J. M.; Stanton, I. N.; Heben, M. J.; Therien, M. J.; Blackburn, J. L. Effect of Solvent Polarity and Electrophilicity on Quantum Yields and Solvatochromic Shifts of Single-Walled Carbon Nanotube Photoluminescence. *J. Am. Chem. Soc.* **2012**, *134* (30), 12485−12491.
(47) Choi, J. H.; Strano, M. S. Solvatochromism in Single-Walled Carbon Nanotubes. *Appl. Phys. Lett.* **2007**, *90* (22), 223114.
(48) Marín, T.; Dulcey, A. E.; Campos, F.; de la Fuente, C.; Acuña, M.; Castro, J.; Pinto, C.; Yañez, M. J.; Cortez, C.; McGrath, D. W.; Sáez, P. J.; Gorshkov, K.; Zheng, W.; Southall, N.; Carmo-Fonseca, M.; Marugán, J.; Alvarez, A. R.; Zanlungo, S. C-Abl Activation Linked to Autophagy-Lysosomal Dysfunction Contributes to Neurological Impairment in Niemann-Pick Type A Disease. *Front Cell Dev Biol.* **2022**, *10*, 844297.

https://doi.org/10.1021/acs.nanolett.3c02502
Nano Lett. 2023, 23, 10687−10695

(49) Kornhuber, J.; Tripal, P.; Reichel, M.; Mühle, C.; Rhein, C.; Muehlbacher, M.; Groemer, T. W.; Gulbins, E. Functional Inhibitors of Acid Sphingomyelinase (FIASMAs): A Novel Pharmacological Group of Drugs with Broad Clinical Applications. *Cell. Physiol. Biochem.* **2010**, *26* (1), 9−20.
(50) Li, X.; Xu, M.; Pitzer, A. L.; Xia, M.; Boini, K. M.; Li, P.-L.; Zhang, Y. Control of Autophagy Maturation by Acid Sphingomyelinase in Mouse Coronary Arterial Smooth Muscle Cells: Protective Role in Atherosclerosis. *J. Mol. Med.* **2014**, *92* (5), 473−485.
(51) McLeland, C. B.; Rodriguez, J.; Stern, S. T. Autophagy Monitoring Assay: Qualitative Analysis of MAP LC3-I to II Conversion by Immunoblot. *Methods Mol. Biol.* **2011**, *697*, 199−206.
(52) Lozano, J.; Menendez, S.; Morales, A.; Ehleiter, D.; Liao, W. C.; Wagman, R.; Haimovitz-Friedman, A.; Fuks, Z.; Kolesnick, R. Cell Autonomous Apoptosis Defects in Acid Sphingomyelinase Knockout Fibroblasts. *J. Biol. Chem.* **2001**, *276* (1), 442−448.
(53) Roxbury, D.; Jena, P. V.; Williams, R. M.; Enyedi, B.; Niethammer, P.; Marcet, S.; Verhaegen, M.; Blais-Ouellette, S.; Heller, D. A. Hyperspectral Microscopy of Near-Infrared Fluorescence Enables 17-Chirality Carbon Nanotube Imaging. *Sci. Rep.* **2015**, *5*, 14167.
(54) Strauss, K.; Goebel, C.; Runz, H.; Möbius, W.; Weiss, S.; Feussner, I.; Simons, M.; Schneider, A. Exosome Secretion Ameliorates Lysosomal Storage of Cholesterol in Niemann-Pick Type C Disease. *J. Biol. Chem.* **2010**, *285* (34), 26279−26288.
(55) Lee, C. Y.; Lesimple, A.; Larsen, A.; Mamer, O.; Genest, J. ESI-MS Quantitation of Increased Sphingomyelin in Niemann-Pick Disease Type B HDL. *J. Lipid Res.* **2005**, *46* (6), 1213−1228.
(56) Horinouchi, K.; Erlich, S.; Perl, D. P.; Ferlinz, K.; Bisgaier, C. L.; Sandhoff, K.; Desnick, R. J.; Stewart, C. L.; Schuchman, E. H. Acid Sphingomyelinase Deficient Mice: A Model of Types A and B Niemann-Pick Disease. *Nat. Genet.* **1995**, *10* (3), 288−293.
(57) Galassi, T. V.; Antman-Passig, M.; Yaari, Z.; Jessurun, J.; Schwartz, R. E.; Heller, D. A. Long-Term in Vivo Biocompatibility of Single-Walled Carbon Nanotubes. *PLoS One* **2020**, *15* (5), e0226791.
(58) Porkka, K.; Koskenvesa, P.; Lundán, T.; Rimpiläinen, J.; Mustjoki, S.; Smykla, R.; Wild, R.; Luo, R.; Arnan, M.; Brethon, B.; Eccersley, L.; Hjorth-Hansen, H.; Höglund, M.; Klamova, H.; Knutsen, H.; Parikh, S.; Raffoux, E.; Gruber, F.; Brito-Babapulle, F.; Dombret, H.; Duarte, R. F.; Elonen, E.; Paquette, R.; Zwaan, C. M.; Lee, F. Y. F. Dasatinib Crosses the Blood-Brain Barrier and Is an Efficient Therapy for Central Nervous System Philadelphia Chromosome-positive Leukemia. *Blood* **2008**, *112* (4), 1005−1012.
(59) Takayama, N.; Sato, N.; O'Brien, S. G.; Ikeda, Y.; Okamoto, S.-I. Imatinib Mesylate Has Limited Activity against the Central Nervous System Involvement of Philadelphia Chromosome-Positive Acute Lymphoblastic Leukaemia due to Poor Penetration into Cerebrospinal Fluid. *Br. J. Hamaetol.* **2002**, *119*, 106−108.
(60) Wang, S.; Li, X.; Chong, S. Y.; Wang, X.; Chen, H.; Chen, C.; Ng, L. G.; Wang, J.-W.; Liu, B. In Vivo Three-Photon Imaging of Lipids Using Ultrabright Fluorogens with Aggregation-Induced Emission. *Adv. Mater.* **2021**, *33* (11), e2007490.
(61) Soria, F. N.; Paviolo, C.; Doudnikoff, E.; Arotcarena, M.-L.; Lee, A.; Danné, N.; Mandal, A. K.; Gosset, P.; Dehay, B.; Groc, L.; Cognet, L.; Bezard, E. Synucleinopathy Alters Nanoscale Organization and Diffusion in the Brain Extracellular Space through Hyaluronan Remodeling. *Nat. Commun.* **2020**, *11* (1), 3440.
(62) Galvan, C.; Camoletto, P. G.; Cristofani, F.; Van Veldhoven, P. P.; Ledesma, M. D. Anomalous Surface Distribution of Glycosyl Phosphatidyl Inositol-anchored Proteins in Neurons Lacking Acid Sphingomyelinase. *MBoC* **2008**, *19* (2), 509−522.
(63) Yang, S. J.; Del Bonis-O'Donnell, J. T.; Beyene, A. G.; Landry, M. P. Near-Infrared Catecholamine Nanosensors for High Spatiotemporal Dopamine Imaging. *Nat. Protoc.* **2021**, *16* (6), 3026−3048.
(64) Schuchman, E. H. Acid Sphingomyelinase, Cell Membranes and Human Disease: Lessons from Niemann-Pick Disease. *FEBS Lett.* **2010**, *584* (9), 1895−1900.
(65) Fan, M.; Sidhu, R.; Fujiwara, H.; Tortelli, B.; Zhang, J.; Davidson, C.; Walkley, S. U.; Bagel, J. H.; Vite, C.; Yanjanin, N. M.; Porter, F. D.; Schaffer, J. E.; Ory, D. S. Identification of Niemann-Pick C1 Disease Biomarkers through Sphingolipid Profiling. *J. Lipid Res.* **2013**, *54* (10), 2800−2814.
(66) Smith, E. L.; Schuchman, E. H. The Unexpected Role of Acid Sphingomyelinase in Cell Death and the Pathophysiology of Common Diseases. *FASEB J.* **2008**, *22* (10), 3419−3431.
(67) Harrington, M. G.; Fonteh, A. N.; Oborina, E.; Liao, P.; Cowan, R. P.; McComb, G.; Chavez, J. N.; Rush, J.; Biringer, R. G.; Hühmer, A. F. The Morphology and Biochemistry of Nanostructures Provide Evidence for Synthesis and Signaling Functions in Human Cerebrospinal Fluid. *Cerebrospinal Fluid Res.* **2009**, *6*, 10.
(68) Fonteh, A. N.; Ormseth, C.; Chiang, J.; Cipolla, M.; Arakaki, X.; Harrington, M. G. Sphingolipid Metabolism Correlates with Cerebrospinal Fluid Beta Amyloid Levels in Alzheimer's Disease. *PLoS One* **2015**, *10* (5), e0125597.
(69) Park, M. H.; Jin, H. K.; Bae, J.-S. Potential Therapeutic Target for Aging and Age-Related Neurodegenerative Diseases: The Role of Acid Sphingomyelinase. *Exp. Mol. Med.* **2020**, *52* (3), 380−389.
(70) Lee, J. K.; Jin, H. K.; Park, M. H.; Kim, B.-R.; Lee, P. H.; Nakauchi, H.; Carter, J. E.; He, X.; Schuchman, E. H.; Bae, J.-S. Acid Sphingomyelinase Modulates the Autophagic Process by Controlling Lysosomal Biogenesis in Alzheimer's Disease. *Journal of Experimental Medicine.* **2014**, *211*, 1551−1570.

NOTE ADDED AFTER ASAP PUBLICATION

This paper was published ASAP on October 27, 2023, with a missing Supporting Information file. The corrected version was reposted on November 21, 2023.

https://doi.org/10.1021/acs.nanolett.3c02502
Nano Lett. 2023, 23, 10687−10695